

Cite this: *RSC Adv.*, 2014, 4, 62532

Palladium nanoparticles supported on natural nanozeolite clinoptilolite as a catalyst for ligand and copper-free C–C and C–O cross coupling reactions in aqueous medium†

Seyed Meysam Baghbanian,^{*a} Horieh Yadollahy,^a Mahmood Tajbakhsh,^b Maryam Farhang^b and Pourya Biparva^c

In this article, Pd⁰-nanoparticles supported on natural nanozeolite clinoptilolite (CP) were successfully synthesized, and the catalytic activity of the nanocatalyst was investigated in C–C and C–O coupling reactions, namely the Sonogashira and Ullmann condensation reactions in an aqueous medium. The nanocatalyst was characterized by various techniques such as powder-XRD, BET, SEM, TEM, HRTEM, TEM-EDS, ICP-OES and XPS. From an electron microscopy (SEM) study it can be inferred that the particles are mostly spherical or of ellipsoidal shape and have diameters ranging from 25 to 80 nm. A HRTEM study reveals that Pd⁰-nanoparticles supported on nanozeolite CP have an average diameter of ~10 nm. The supported palladium nanoparticles showed excellent catalytic activity in the synthesis of aryl alkynes and diaryl ethers in high yields. In addition, the nanocatalyst could be recycled and reused several times without significant loss of catalytic activity.

Received 28th September 2014

Accepted 13th November 2014

DOI: 10.1039/c4ra11411f

www.rsc.org/advances

1. Introduction

Clinoptilolite (CP) is one of the most plentiful and economically important natural zeolites.¹ Its crystalline structure contains three types of channels confined by tetrahedral ring systems, which are monoclinic frameworks consisting of a ten member as well as two eight-member rings.² The channels are occupied by water molecules and compensating cations, which neutralize the anionic charge of the framework. They are used for many applications such as chemical sieves,³ gas absorbers,⁴ feed additives,⁵ odor control agents, water filters and especially in agriculture, environmental protection and even medicine.⁶ In a recent study, it was proved that they can be employed in organic synthesis as a catalyst.⁷ Therefore, investigation of the use of “CP” as a reliable catalyst support seems to be worth studying. So, we considered the applicability of this valuable multipurpose compound as a metal catalyst support due to its outstanding characteristics, including high and adjustable acidity, well defined pore structures with channels and cavities of molecular dimensions and high ion-exchange capabilities.⁸

Palladium-catalyzed cross-coupling for the C–C and C–O bonds forming reactions have increased exponentially over the years because of their vast applications in the preparation of notable compounds. Various Pd complexes have been applied as homogeneous or heterogeneous catalysts, but limitations in recovery of expensive palladium and separation of the products in industrial applications are still a challenge.⁹ To solve these problems, palladium has been supported on materials such as activated carbon,¹⁰ zeolites and molecular sieves,¹¹ metal oxides (SiO₂,^{12a} TiO₂ (ref. 12b)), clays,¹³ alkali and alkaline earth salts,¹⁴ organic polymers,¹⁵ mesoporous silica,¹⁶ capsules,¹⁷ and basic metal phosphates (apatite).¹⁸ Among them, zeolites^{11a–e} and natural zeolites^{11f,g} have been widely used as inorganic supports to provide an efficient way for solving the problems of separation and reusability of catalyst, as well as preventing the aggregation of nanoparticles.^{19,20} However, natural zeolites hold some key advantages over their synthetic analogues due to their natural characteristics and constituents, much less processing cost, availability, greater thermal stability and better resistance to acid environments.²¹ In this regard, natural nanozeolite CP has been investigated as a proper host providing large cavities to encapsulate metal species.^{11f,g}

The Sonogashira reaction has gained much interest due to its wide range of applicability in the synthesis of important organic molecules through the C–C bond formation.²² One example is the formation of new carbon (sp²)–carbon (sp) bonds leading to conjugated acetylenic compounds which is frequently employed in the synthesis of natural products

^aDepartment of Chemistry, Ayatollah Amoli Branch, Islamic Azad University, Amol, Iran. E-mail: s.m.baghbanian@iauamol.ac.ir; Fax: +98-1143217071; Tel: +98-1143217000

^bFaculty of Chemistry, Mazandaran University, Babolsar, 47415, Iran

^cDepartment of Basic Sciences, Sari Agricultural Sciences and Natural Resources University, P. O. Box 578, Sari, Iran

† Electronic supplementary information (ESI) available. See DOI: 10.1039/c4ra11411f

including enediyne antibiotics, as well as in the preparation of liquid crystals, conducting dendrimers and conjugated polymers or nanostructures.²³ Generally, the Sonogashira coupling reaction is carried out in the presence of palladium, ligands, combined with a co-catalytic amount of CuI as the catalytic system.²⁴ Cu(I) acetylide is obtained *in situ* with the presence of CuI can undergo oxidative homocoupling reaction of alkynes.²⁵ Furthermore, many ligands are air sensitive and expensive, resulting in significant limits on their synthetic applications. Thus, development of a simple, eco-benign and low cost protocol, using a neutral and reusable catalyst for one-pot Sonogashira cross-coupling reaction without any ligand and co-catalyst still remains as an attractive goal for researchers.

In addition, diaryl ethers are useful compounds that having properties, such as antibacterial, anti-inflammatory, antifungal and herbicidal activity.²⁶ Also, many diaryl ethers are important structural motifs found in a variety of naturally occurring medicinally active compounds including riccardin B,²⁷ tetramethylmagnolamine,²⁸ K-13,²⁹ piperazinomycin³⁰ and perrottetia.³¹ Ullmann type coupling is one of the most important methods for the preparation of diaryl ethers. In the recent years, several improved protocols for O-arylation of phenols have been reported using palladium or copper as the catalyst. Although these methods are effective, but most of them still have some drawbacks resulting in significant limits on their synthetic applications such as high reaction temperatures, use of toxic solvents and stoichiometric amounts of metal reagents, employing sensitive and costly ligands and moderate yields.^{32–34} On the other hand, many of palladium-reactions described the use of organic bromides, iodides and triflates for the preparation of diaryl ethers. However, chlorides are generally unreactive³⁵ and the coupling of aryl chlorides with phenols have been rarely described in the literature.³⁶ Thus, development of a simple, eco-benign and low cost protocol using a natural and reusable catalyst for the clean synthesis of diaryl ethers still remains as an attractive subject for research.

In continuation of our recent efforts on introducing novel methodologies, in particular, study related to the use of nanozeolite clinoptilolite as a heterogeneous catalyst,³⁷ herein we report the successful synthesis of Pd⁰-nanoparticles supported

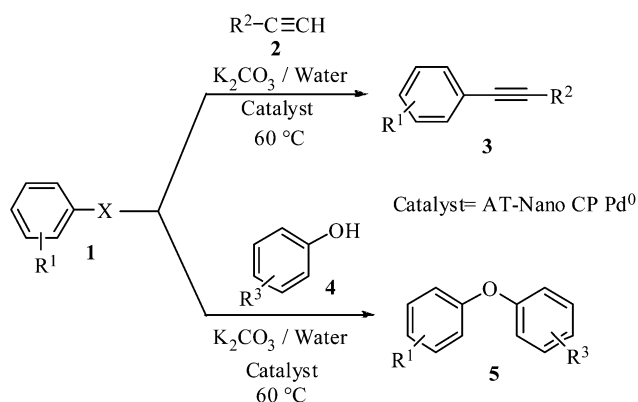
on the natural nanozeolite CP as an excellent catalyst for the Sonogashira and Ullmann type coupling reactions and in aqueous medium (Scheme 1).

2. Results and discussion

The nanozeolite CP was prepared according to a simple method developed recently by our group³⁷ and subsequently activated with 4 M sulfuric acid. The activated nanozeolite CP was designated as AT(activated)-Nano CP. AT-Nano CP was taken into a round-bottom flask, and an aqueous solution of K₂PdCl₄ was added slowly under vigorous stirring condition to give AT-Nano CP-[PdCl₄]²⁻. Finally, AT-Nano CP-[PdCl₄]²⁻ composite was dispersed in dry ethanol and then hydrazine hydrate was added to prepare AT-Nano CP-Pd⁰. Stepwise preparation of AT-Nano CP-Pd⁰ is illustrated in Fig. 1.

2.1. Characterization of support

2.1.1. X-ray diffraction. X-ray diffraction (XRD) is a versatile and non-destructive technique for the determination of the crystallographic structure of materials and analyzing structural properties of the phases. Therefore, X-ray diffraction patterns were recorded for AT-Nano CP and Nano CP-Pd⁰ (Fig. 2). XRD pattern of AT-Nano CP shows peaks at $2\theta = 12.76^\circ$, 21.74° , 27.46° and 35.92° , which agrees with the natural zeolite clinoptilolite data (JCPDS 00-025-1349) (Fig. 2a). AT-Nano CP-Pd⁰ exhibited broad peaks at $2\theta = 39.88^\circ$, 46.42° , 68.04° , 82.1° and 87.28° corresponding to diffraction lines (111), (200), (220), (311) and (222), respectively. The diffraction peaks in this pattern clearly indicate the face-centered cubic (fcc) lattice of metallic Pd (Fig. 2b). The average crystallite size for Pd⁰-nanoparticles was calculated to be below 10 nm based on the strongest intensity of (111) peak using the Debye–Scherrer's formula $D = 0.89\lambda/(\beta \cos \theta)$; where D is the grain size, β is the angular line width of half-maximum intensity in radians, θ is Bragg's diffraction angle and λ is the X-ray wavelength used. The XRD pattern of the recovered catalyst after 8 cycles is as same as the fresh catalyst but the peaks intensity has been decreased (Fig. 2c). This phenomenon shows that the Pd⁰-nanoparticles is not changed during C–C and C–O cross coupling reactions. The



Scheme 1 C–C and C–O cross coupling reactions.

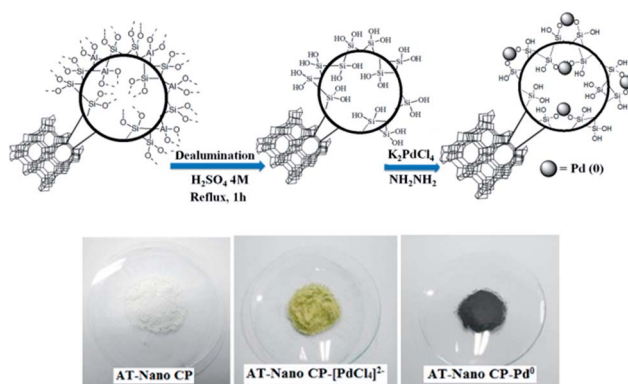


Fig. 1 Schematic representation of the incorporation of tetrahedral coordinated Pd⁰ into AT-Nano CP.

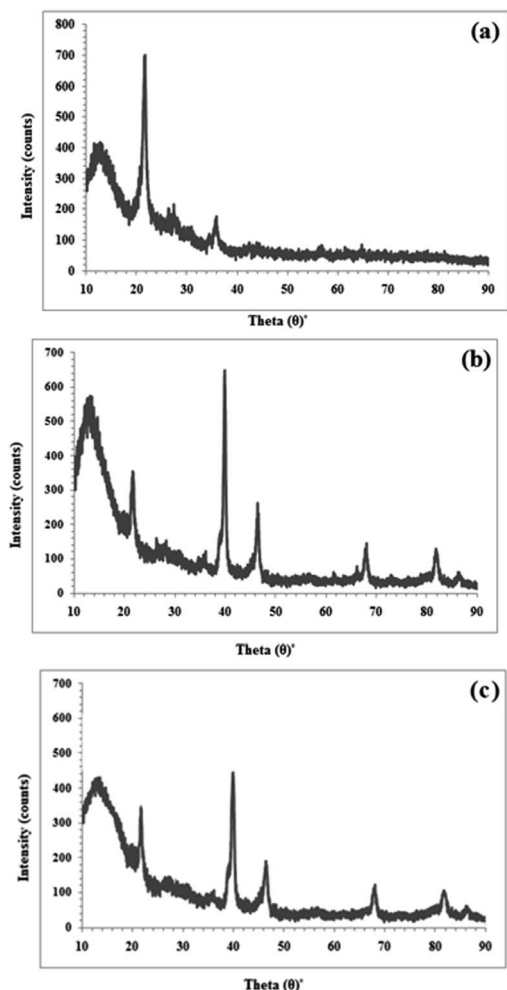


Fig. 2 XRD patterns of (a) AT-Nano CP, (b) AT-Nano CP-Pd⁰ and (c) AT-Nano CP-Pd⁰ recovered after 8th cycles.

amount of loaded palladium on AT-Nano CP surface was estimated by inductively coupled plasma-optical emission spectrometry (ICP-OES) to be 0.2 mmol g⁻¹.

2.1.2. Specific surface area and pore size distribution. The N₂ adsorption-desorption isotherms for Nano CP, AT-Nano CP, AT-Nano CP-Pd⁰ and AT-Nano CP-Pd⁰ after eight cycles were measured and the specific surface area (*S*), the total pore and micropore volumes (*V*_{tot} and *V*_{mic}), and the average pore diameter (*D*) were calculated using the adsorption data. The specific surface area (*S*_{BET}) was calculated (Fig. S1, ESI†) by applying the Brunauer-Emmett-Teller (BET) method, and the mesopore surface area *S*_{BJH} and the mesopore volume *V*_{BJH} were calculated for Nano CP, AT-Nano CP, AT-Nano CP-Pd⁰ and AT-Nano CP-Pd⁰ after eight cycles using the Barrett-Joyner-Halenda (BJH) method (Table 1). According to the Brunauer, Deming, Dering and Teller (BDDT) classification, characteristic of mesoporous solids,³⁸ all the materials displayed typical type IV isotherm with an H₃ hysteresis loop at *P*/*P*₀ ~ 0.984. The Nano CP with average pore diameters ~12.19 nm contained a specific surface area of 49.7 m² g⁻¹ and a specific pore volume of 0.15 cm³ g⁻¹. Increase in the specific surface area from 49.7 m² g⁻¹ to 55.6 m² g⁻¹ and

Table 1 Surface properties of different nanozeolite based support/catalysts

Sample	Specific surface area [m ² g ⁻¹]		Specific pore volume [cm ³ g ⁻¹]		Pore diameter [nm]	
	<i>S</i> _{BET}	<i>S</i> _{BJH}	<i>V</i> _{tot} (BET)	<i>V</i> (BJH)	<i>D</i> _{av}	<i>D</i> (BJH)
Nano CP	49.7	45.68	0.15	0.15	12.19	1.64
AT-Nano CP	55.6	39.52	0.11	0.1	8.05	1.21
AT-Nano CP-Pd ⁰	48.8	35.46	0.09	0.08	8.49	1.38
AT-Nano CP-Pd ^{0a}	35.9	30.54	0.05	0.04	14.48	1.49

^a Eight cycles reused in Sonogashira coupling reaction.

a slight decrease in the specific pore volume from 0.15 cm³ g⁻¹ to 0.12 cm³ g⁻¹ observed after the activation of Nano CP might be due to the leaching of Al from sites of the zeolite matrix and decationation during acid activation. Furthermore, decrease of the average pore diameter from 12.19 nm to 8.05 nm after acid treatment may be due to break of some bigger pores to generate smaller ones.³⁹ The BJH curves of nitrogen desorption display descent distribution of pore volume in the mesoporous section (1–100 nm). The decrease of the pore diameter from 1.64 nm to 1.21 nm and the pore volume from 0.15 cm³ g⁻¹ to 0.1 cm³ g⁻¹ was observed after the activation of Nano CP. According to the analysis of the data listed in Table 1, the specific surface area and the specific pore volume were decreased after supporting Pd⁰-nanoparticles could be due to clogging of some pores by Pd⁰-nanoparticles. Since that a sudden change has not occurred in the specific pore volume and surface area of AT-Nano CP after Pd⁰ encapsulation further approves that pores of AT-Nano CP are not clogged by Pd⁰ nanoparticles larger than the pore size of AT-Nano CP. On the other hand, increase of average pore diameter after loading Pd⁰ from 8.05 nm to 8.49 nm can be because of fracture and demolition of some smaller pores to generate bigger ones during the establishment of Pd⁰ nanoparticles into the pores (ESI†). The BJH pore size distribution curves (Fig. S1(l), ESI†) of the recovered catalyst was slightly broader compared to that of the fresh catalyst, indicating the formation of large pores because of breakage in the pore walls.³⁹ This resulted in the decrease of the peak sharpness in XRD pattern (Fig. 2c) of the catalyst after 8th cycle in agreement with similar systems reported in the literature.³⁹ The N₂ adsorption-desorption isotherms of AT-Nano CP-Pd⁰ after being used repeatedly eight times (Fig. S1(d), ESI†) demonstrate the damage of the mesoporous structure, leading to an abrupt decrease in surface area and pore volume (Table 1).

2.1.3. SEM investigation. The structural and morphological characterizations of Nano CP, AT-Nano CP and AT-Nano CP-Pd⁰ were performed using SEM (Fig. 3). Comparison of the SEM images of Nano CP (Fig. 3a), AT-Nano CP (Fig. 3b) and AT-Nano CP-Pd⁰ (Fig. 3c) shows that the morphological features such as the spherical or ellipsoidal shape and non-aggregation characteristics are not changed significantly. SEM image of the AT-Nano CP-Pd⁰ also showed the average particle size to be in the range of 25–80 nm.

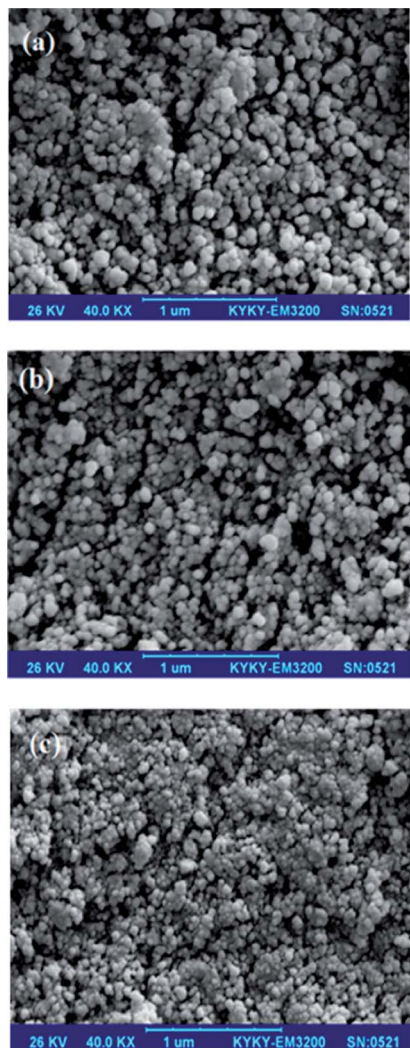


Fig. 3 SEM images of (a) Nano CP, (b) AT-Nano CP and (c) AT-Nano CP-Pd⁰.

2.1.4. TEM, HRTEM and TEM-EDS analyses. The TEM images of AT-Nano CP (Fig. 4a) and AT-Nano CP-Pd⁰ (Fig. 4b) confirmed the distribution of Pd⁰-nanoparticles in the mesoporous structure of AT-Nano CP. The Pd⁰-nanoparticles have spherical or ellipsoidal shapes, uniformly distributed and anchored along the heterogeneous mesoporous surface of AT-Nano CP with average sizes of below 10 nm (Fig. 4c), which is quite consistent with the data obtained from the XRD analysis. TEM study indicates that few Pd⁰-nanoparticles were found to be larger than the pore size of AT-Nano CP, which could be due to the presence of Pd⁰-nanoparticles on the outer surface of AT-Nano CP rather than inside the pores. The HRTEM image of Pd⁰-nanoparticles reveals the reticular lattice planes can be seen inside the nanoparticles, indicating the crystal structure of clinoptilolite. TEM-EDS data for AT-Nano CP revealed the presence of the expected elements in the structure of zeolite, namely C, O, Si and small amount of Al (Fig. 4d). The low intensity of Al peak might be due to the leaching of Al from sites of the zeolite matrix during acid activation (Fig. 4d). Furthermore, TEM-EDS

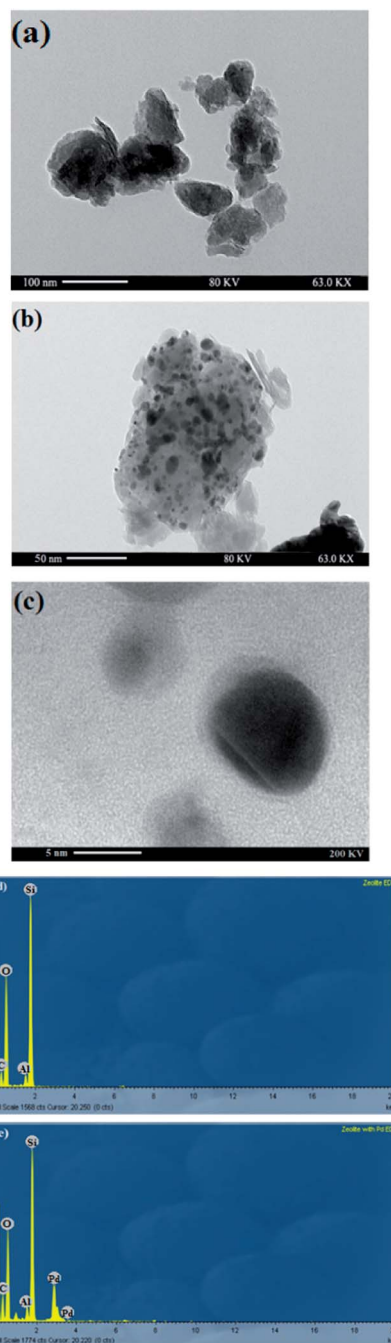


Fig. 4 TEM images of (a) AT-Nano CP and (b) AT-Nano CP-Pd⁰. (c) HRTEM image of AT-Nano CP-Pd⁰. TEM-EDS data of (d) AT-Nano CP and (e) AT-Nano CP-Pd⁰.

analysis of AT-Nano CP Pd⁰ also indicates the presence of Pd⁰-nanoparticle on the well-tuned pores of modified zeolite together with other elements of zeolite (Fig. 4e).

2.1.5. X-ray photoelectron spectroscopy (XPS) analysis. Fig. 5a shows the XPS survey scans of AT-Nano CP-Pd⁰ sample displaying the signals of the elements on their surfaces. The more intense signals are related to the O, Si, Al and Pd elements in the CP framework. The XPS spectrum exhibited three peaks in the Si2p region. The weaker signal at energy binding of

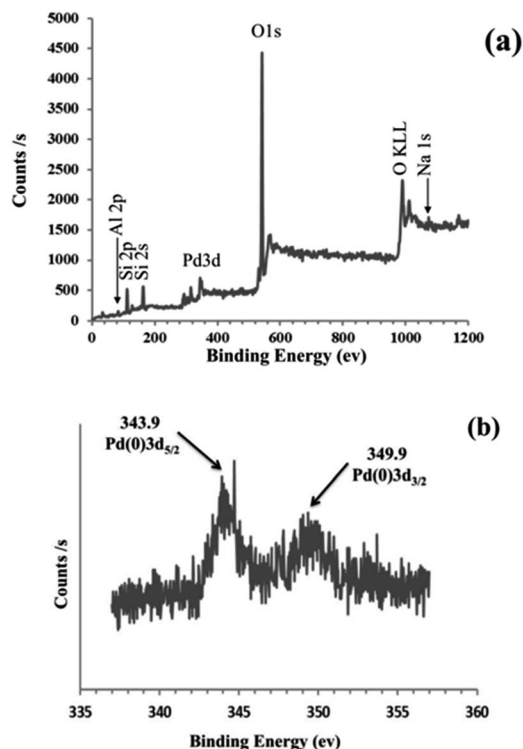


Fig. 5 XPS survey spectra of AT-Nano CP-Pd⁰ (a), the high resolution scan of Pd 3d bands (b).

101.07 eV can be related to the signal of Si2p in Na-SiO₃.^{40,41} The two peaks observed at binding energy of 113.03 and 162.38 eV could be attributed to the signal of Si2p in SiO₂. The survey-scan XPS spectrum of AT-Nano CP-Pd⁰ reveals two prominent bands at 343.9 eV and 349.9 eV, which can readily be assigned to Pd(0) 3d_{5/2} and 3d_{3/2} bands, respectively (Fig. 5b). On the other hand, the signal of Na ions is observed in the Na1s region at 1073.0 eV, corresponding to the binding energy of Na in Na₂O indicating that the bonding of Na ions to O ions in the clinoptilolite matrix.⁴⁰

2.2. Sonogashira coupling reaction catalyzed by AT-Nano CP-Pd⁰

The AT-Nano CP-Pd⁰ catalyzed Sonogashira coupling reaction between phenylacetylene and iodobenzene was chosen as a model reaction to evaluate the effects solvent, base, temperature and quantity of catalyst. Optimization conditions are summarized in Table 2. For the initial study, water was used as solvent and K₂CO₃ as base in the presence of 0.001–0.004 g AT-Nano CP-Pd⁰ at 60 °C. The best results were obtained using 3 mg of the catalyst (Table 2, entry 4). By increasing the quantity of the catalyst, no significant improvement in yield was observed (Table 2, entry 5). After achieving a high yield in water, studies focused on the effect of various bases such as NaOH, K₃PO₄ and Et₃N on the model reaction (Table 2, entries 6–8). Among the bases examined, K₂CO₃ was the more effective base in this reaction to perform a high yield of the product **3a** (Table 2, entry 4). The model reaction was carried out in various

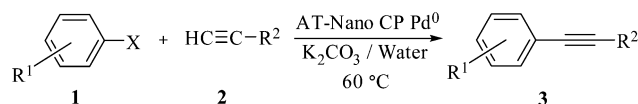
Table 2 Effect of the loading catalyst and different bases on the catalytic activity of AT-Nano CP-Pd⁰ in the Sonogashira reaction^a

Entry	Solvent	Base	Catalyst [g]	Temp. [°C]	Time [h]	Yield [%]
1	H ₂ O	K ₂ CO ₃	—	60	2	—
2	H ₂ O	K ₂ CO ₃	0.001	60	3	70
3	H ₂ O	K ₂ CO ₃	0.002	60	2	88
4	H ₂ O	K ₂ CO ₃	0.003	60	1	95
5	H ₂ O	K ₂ CO ₃	0.004	60	1	95
6	H ₂ O	NaOH	0.003	60	1	60
7	H ₂ O	K ₃ PO ₄	0.003	60	1	75
8	H ₂ O	Et ₃ N	0.003	60	1	40
9	H ₂ O	K ₂ CO ₃	0.003	25	1	40
10	H ₂ O	K ₂ CO ₃	0.003	45	1	75
11	H ₂ O	K ₂ CO ₃	0.003	100	1	95
12	EtOH	K ₂ CO ₃	0.003	60	2	88
13	DMSO	K ₂ CO ₃	0.003	60	2	82
14	DMF	K ₂ CO ₃	0.003	60	2	80
15	Toluene	K ₂ CO ₃	0.003	60	3	60

^a Reaction conditions: phenylacetylene (1 mmol), iodobenzene (1 mmol), water (5 mL), and 1.5 mmol base.

solvents such as EtOH, DMF, DMSO and toluene instead of water (Table 2, entries 12–15). Interestingly, changing the solvent did not provide any improved yields under optimized condition. Various temperatures ranging from 25 to 100 °C (Table 2, entries 4, 9–11) were examined and it was found that the Sonogashira coupling reaction proceeds efficiently at 60 °C in terms of reaction rate and isolated yield (Table 2, entry 4).

Due to the remarkable results on the optimized reaction conditions using AT-Nano CP-Pd⁰ as catalyst, K₂CO₃ as base in water encouraged us to investigate the conceivability of this methodology for a wide range of substituted aryl halides. Results demonstrate that all substituted aryl halides (chlorides, bromides and iodides) reacted with terminal alkynes in the presence of K₂CO₃ as base in water to afford the corresponding cross-coupling product in good to excellent yields (Table 3). Aryl halides substituted with electron-withdrawing groups, in comparison with electron-donating substituents, gave better conversions in shorter reaction times. The reactions of aryl iodides with phenylacetylene were fast and excellent coupling yields were obtained (Table 3, entries 1–4 and 11). To extend the scope of present method, the coupling of various aryl bromides with phenylacetylene were investigated. As can be seen in Table 3, high catalytic activity was observed in the coupling reactions of aryl bromides with phenylacetylene (Table 3, entries 5–7). The reactions of phenylacetylene with aryl chlorides were carried out in the presence of AT-Nano CP-Pd⁰ under optimal reaction conditions to afford good yields of corresponding products



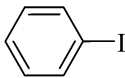
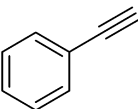
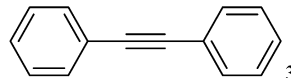
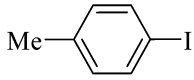
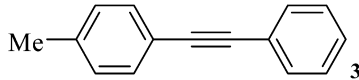
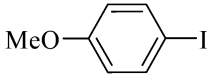
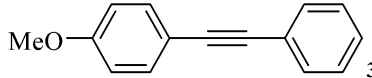
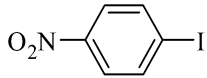
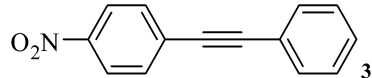
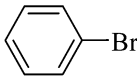
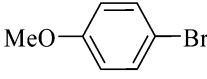
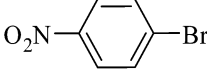
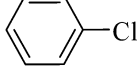
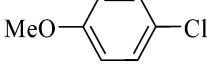
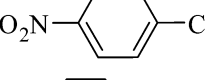
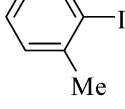
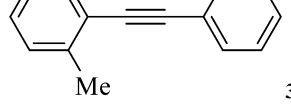
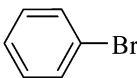
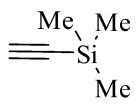
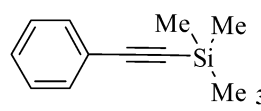
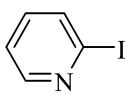
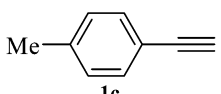
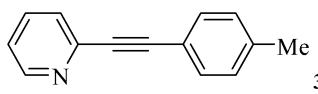
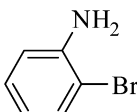
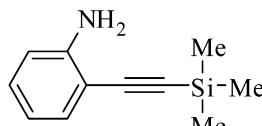
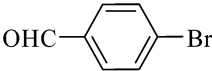
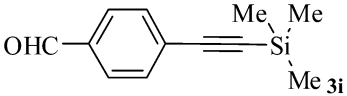
Entry	Aryl halide	Alkyne	Products	Time [h]	Yield ^b [%]
1		 1a	 3a	1	95
2		1a	 3b	2	92
3		1a	 3c	2	89
4		1a	 3d	1	94
5		1a	3a	2	90
6		1a	3b	3	88
7		1a	3d	1	92
8		1a	3a	3	85
9		1a	3c	2	80
10		1a	3d	2	89
11	 Me	1a	 Me 3e	2	85
12		 1b	 Me Me Si Me 3f	2	95
13		 1c	 Me 3g	2	75
14		1b	 NH ₂ Me Si-Me Me 3h	5	40

Table 3 (Contd.)

$ \begin{array}{c} \text{R}^1 \\ \\ \text{C}_6\text{H}_4\text{-X} \\ \text{1} \end{array} + \text{HC}\equiv\text{C-R}^2 \xrightarrow[60^\circ\text{C}]{\text{AT-Nano CP Pd}^0, \text{K}_2\text{CO}_3 / \text{Water}} \begin{array}{c} \text{R}^1 \\ \\ \text{C}_6\text{H}_4\text{-C}\equiv\text{C-R}^2 \\ \text{3} \end{array} $					
Entry	Aryl halide	Alkyne	Products	Time [h]	Yield ^b [%]
15		1b		3	92

^a Reaction conditions: aryl halides (1 mmol), phenylacetylene (1 mmol), water (5 mL), K₂CO₃ (1.5 mmol) and the catalyst (3 mg, containing 6×10^{-4} mmol, 6.3×10^{-5} g of Pd), 60 °C. ^b Yields of purified products.

(Table 3, entries 8–10). 2-Iodopyridine as a heteroaryl halide tolerated well in this reaction and a moderate yield of the desired products was obtained (Table 3, entry 13). In further studies, the reactions of ethynyltrimethylsilane with bromobenzene and aryl bromide substituted with an electron-withdrawing group *i.e.*, –CHO (Table 3, entries 12 and 15) proceed smoothly, while electron-donating substitute group, *i.e.*, –NH₂ (Table 3, entry 14) disfavored the reaction.

2.3. Ullmann coupling reaction catalyzed by AT-Nano CP–Pd⁰

After the successful application of AT-Nano CP–Pd⁰ in Sonogashira coupling reaction, the efficacy of this catalyst in the O-arylation of phenols was examined. To optimize the reaction conditions, the reaction of iodobenzene with phenol was selected as the model reaction in an aqueous medium. In this reaction, the same conditions as Sonogashira reaction was used, and desired product was obtained in 98% isolated yield (Table 4, entry 1). Therefore, we have chosen the same reaction conditions for Ullmann condensation reaction as that of Sonogashira reaction (ESI†).

To develop the scope of the methodology using AT-Nano CP–Pd⁰ for O-arylation of phenols, the coupling of various substituted aryl halides with phenols have been investigated, and the results are summarized in Table 4. Although, the catalytic activity of AT-Nano CP–Pd⁰ is dependent on the substituent of aryl halides and phenols used in the reaction in all cases, diaryl ethers were obtained in excellent yields (Table 4, entries 2–14). Besides, naphthols coupled to aryl halides smoothly under reaction conditions to afford the desired products in good yields (Table 4, entries 15–17).

The recyclability of the AT-Nano CP–Pd⁰ catalyst was investigated for Sonogashira (Fig. 6a) and Ullmann coupling reaction (Fig. 6b) under the optimized reaction conditions. The catalyst was recovered by filtration technique after each experiment and washed twice with hot distilled water (2 mL) and ethanol (2 mL). The recovered catalyst was used repeatedly eight runs in the water-medium Sonogashira coupling reaction and six runs in the Ullmann coupling reaction without any significant loss of

catalytic activity. The strong interaction of Pd⁰ nanoparticles with the zeolite surface could be the reason for the repetitive use of the catalyst in a greater number of catalytic runs with high efficiency.

To confirm the heterogeneous nature of the catalyst, leaching of Pd⁰ species was investigated by premixing AT-Nano CP–Pd⁰ in water at 60 °C for 8 h that is a time longer than the usual reaction time. Then, the catalyst was removed by filtration and all of the reagents (iodobenzene, phenylacetylene and K₂CO₃) were added to the corresponding solution and allowed to react the required period of time (2 h). The result showed no desired product was formed, indicating no catalytically active Pd remained in the filtrate. However, it is known that this test alone does not prove that reaction proceeds truly heterogeneously. Therefore, palladium leaching into the reaction mixture was also studied with ICP-AES which indicated that no palladium metal had leached out from the catalyst surface.

2.4. Comparison with other reported systems

To show the merit of the current protocol for the synthesis of aryl alkynes and diaryl ethers, the results obtained for Sonogashira reaction of phenylacetylene with phenyl halides and Ullmann type reaction of phenol with phenyl halides were compared with some of those reported in the literature using other catalysts (Table 5). Among the heterogeneous catalysts in Table 5 for Sonogashira reaction, the present method comparatively affords a truly green process using water as reaction media and separable nanocatalyst with high yield of the product in shorter reaction time (Table 5, entry 10). Although, other catalysts gave high yield of the product but they suffer from drawbacks such as using synthesized support (Table 5, entries 1, 2, 4–6 and 9), using organic solvents (Table 5, entries 1–5 and 9), high temperatures (Table 5, entries 1–6 and 8) and long reaction times (Table 5, entries 1–8) or using mw irradiation (Table 5, entry 9). Moreover, most phenyl halides were not competent substrates with these systems comparing entry 10 with entries 1–9 and entry 17 with entries 11, 12 and 14–16. For the Ullmann type reaction, although, other catalysts afford high yield of the product, they need organic solvent (Table 5, entries

Table 4 AT-Nano CP-Pd⁰ catalyzed O-arylation of phenols with aryl halides^a

Entry	Aryl halides	Phenol	Product	Time [h]	Yield ^b [%]
1				1	98
2				3	92
3				3	88
4				3	90
5				4	85
6				1	98
7				1	95
8				2	90
9				2.5	92
10				4	88
11				2	92
12				3	80

Table 4 (Contd.)

Entry	Aryl halides	Phenol	Product	Time [h]	Yield ^b [%]
13		4a	5e	4	90
14		4a	5f	2	75
15		4a		10	65
16		4a	5i	12	60
17		4a	5i	14	60

^a Reaction conditions: aryl halides (1 mmol), phenols (1 mmol), water (5 mL), K₂CO₃ (1.5 mmol) and the catalyst (3 mg, containing 6×10^{-4} mmol, 6.3×10^{-5} g of Pd), 60 °C. ^b Yields of purified products.

11, 12 and 14–16), higher temperature (Table 5, entries 12–16) and long reaction times (Table 5, entries 11, 12 and 14–16). However, compare with other catalysts, the present catalytic

system for Sonogashira and Ullmann type reactions, exhibited higher activity with lower amount of catalyst, without using any co-catalyst and ligand in the synthesis of desired products under green and mild reaction conditions (Table 5, entries 10 and 17).

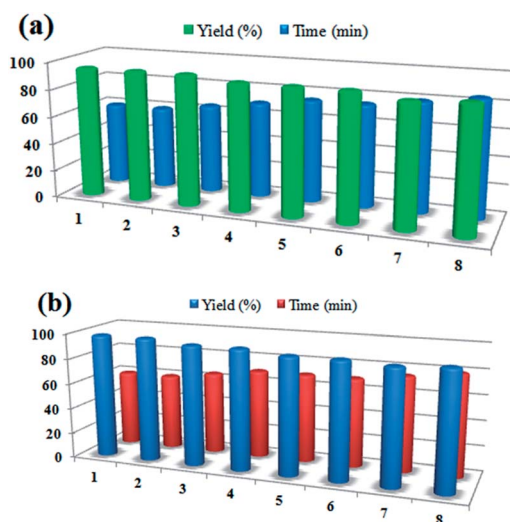


Fig. 6 Recyclability of the catalyst in (a) Sonogashira coupling reaction; reaction conditions: iodobenzene (1 mmol), phenylacetylene (1 mmol), water (5 mL), K₂CO₃ (1.5 mmol) and the catalyst (3 mg, containing 6×10^{-4} mmol, 6.3×10^{-5} g of Pd), 60 °C. (b) Ullmann coupling reaction; reaction conditions: iodobenzene (1 mmol), phenol (1 mmol), water (5 mL), K₂CO₃ (1.5 mmol) and the catalyst (3 mg, containing 6×10^{-4} mmol, 6.3×10^{-5} g of Pd), 60 °C.

3. Experimental

3.1. Reagents and materials

All reagents were prepared from analytical reagent grade chemicals unless specified otherwise and purchased from Merck Company. The raw zeolite material was an Iranian commercial Clinoptilolite (Afrandtooska Company) obtained from deposits in the region of Semnan (ca. 1 % per kg).

3.2. Instrumentation

The X-ray powder diffraction (XRD) of the catalyst was carried out on a Philips PW 1830 X-ray diffractometer with Cu K α source ($\lambda = 1.5418$ Å) in a range of Bragg's angle (10–90°) at room temperature. N₂ sorption measurement was performed using Belsorp mini II at 273 K. Prior to the measurements, all the samples were degassed at 393 K in a vacuum line overnight. The specific surface area and pore volume were calculated with the Brunauer–Emmett–Teller (BET) method, and the pore size distribution was expected with desorption branch based on the Barrett–Joyneer–Halenda (BJH) model. Scanning electron microscope (SEM) pictures were taken using KYKY-EM3200

Table 5 Comparison of activity of different catalysts in the Sonogashira and Ullmann type coupling reactions

Reaction	Entry	Catalyst [mol%]	Reaction conditions	Time [h], Ar-X	Yield [%], Ar-X	Ref.
				X = Cl/Br/I	X = Cl/Br/I	
Sonogashira reaction ^a	1	[Pd(NH ₃) ₄] ²⁺ /Y zeolite [1]	DMF/H ₂ O, Et ₃ N, 80 °C	—/3/3	—/45/100	42
	2	Pd(NO ₃) ₂ /NaA zeolite [1]	DMF/H ₂ O, Na ₂ CO ₃ , 80 °C	—/12/—	—/91/—	43
	3	Pd ⁰ –Mont. [0.07]	CH ₃ CN, Et ₃ N, 82 °C	—/—/3	—/—/90	44
	4	Pd–MCM [0.6]	EtOH, K ₂ CO ₃ , 80 °C	—/12/10	—/72/78	45
	5	Fe ₃ O ₄ @PPh ₂ Pd(OAc) ₂ [0.5]	DMF, K ₂ CO ₃ , 100 °C	—/6/6	—/79/95	46
	6	Nano Pd/ZnO [9 mg]	H ₂ O, K ₂ CO ₃ , 90 °C	—/—/7	—/—/98	47
	7	Pd NPs [2]	H ₂ O, K ₂ CO ₃ , 60 °C	—/—/5	—/—/89	48
	8	Pd(0)/MCoS [0.2]	H ₂ O, Et ₃ N, 80 °C	44/10/6	12/82/94	49
	9	Pd/SiO ₂ [0.5 wt%]	DMF, Et ₃ N, MW	15 min	—/81/83	12a
	10	AT-Nano CP–Pd ⁰ [0.06]	H ₂ O, K ₂ CO ₃ , 60 °C	3/2/1	85/90/95	This work
Ullmann type reaction ^b	11	[(Cinnamyl)PdCl] ₂ [0.025]	Toluene/DME, K ₃ PO ₄ , r.t.	16	—/91/—	50
	12	Pd(OAc) ₂ , ligand [0.1]	Toluene, K ₃ PO ₄ , 120 °C	20	86 ^a	51
	13	Fe ₃ O ₄ @PPh ₂ –Pd ⁰ [1.5]	H ₂ O, K ₂ CO ₃ , 80 °C	3.5/2/1.5	83/90/93	34
	14	CuO NPs [5]	DMSO, KOH, 110 °C	15	Nr/40/93	52
	15	Silica Cu(II) [5]	DMSO, KF, 130 °C	16	—/72/92	53
	16	Ferrous chamosite [25 mg]	DMF, K ₂ CO ₃ , 110 °C	12	35/55/97	54
	17	AT-Nano CP–Pd ⁰ [0.06]	H ₂ O, K ₂ CO ₃ , 60 °C	3/2.5/1	85/92/98	This work

^a Sonogashira reaction: phenylacetylene and phenyl halides. ^b Ullmann type reaction: phenol and phenyl halides.

microscope (acceleration voltage 26 kV). Transmission electron microscopy (TEM) experiments were conducted on a JEOL-2100 microscope operated at 200 KV. The TEM model Samples are sonicated by mixing with 95% ethanol for 30 min, and subsequently dropped onto copper grids coated with carbon film, and dried thoroughly in an electronic drying cabinet at a temperature of 25 °C and relative humidity 45%. The chemical composition and crystallinity analysis of the samples are characterized using a high-resolution transmission electron microscopy (HRTEM; JEOL-2100) equipped with an energy-dispersive X-ray spectrometer (EDS, INCA) operated at 200 KV. X-ray photoelectron spectra (XPS) was recorded on a BESTEC GmbH-8025 spectrometer using a Mg K α ($h\nu = 1253.6$ eV) and Al K α ($h\nu = 1486.6$ eV) X-ray source. The metal content in the materials was determined using Inductively Coupled Plasma (ICP) in a Philips PU-70000 sequential spectrometer equipped. ¹H, ¹³C NMR spectrum was recorded on a BRUKER DRX-400 AVANCE spectrometer.

3.3. Catalyst preparation

3.3.1. Preparation of AT-Nano CP. The nanozeolite clinoptilolite was converted to the homoionic Na⁺-exchanged form by stirring in 2 M NaCl solution for about 24 h, and then the Na⁺-nanozeolite clinoptilolite was filtrated and washed with distilled water (50 mL) two times. The Na⁺-nanozeolite was dried in an oven at 100 °C. Then, the Na⁺-nanozeolite clinoptilolite (5 g) was taken into a 250 mL round bottom flask and 100 mL 4 M sulfuric acid was added to it. The flask mixture was refluxed for 1 h. After cooling, the supernatant was discarded and the activated nanozeolite clinoptilolite was repeatedly washed with deionised water (250 mL) until the solution became neutral and finally dried in oven at 80 °C overnight to

obtain the white solid product. The activated nanozeolite clinoptilolite was designated as AT-Nano CP.

3.3.2. Preparation of AT-Nano CP–Pd⁰. One gram of AT-Nano CP was taken into a 100 mL round bottom flask and 20 mL (0.8 mmol) aqueous solution of K₂PdCl₄ was added slowly under vigorous stirring condition. The resulting mixture was stirred for 6 h at room temperature and then the solvent was evaporated *in vacuo* to obtain AT-Nano CP–[PdCl₄]^{2–}. 0.5 gram of dry AT-Nano CP–[PdCl₄]^{2–} was dispersed in 20 mL dry ethanol in a 100 mL round bottom flask and then 20 mL of hydrazine hydrate was added slowly over 20 min under constant stirring condition. The reaction started immediately, and the color changed from yellow to black (Fig. 1), due to conversion of Pd(II) into Pd⁰-nanoparticles. The black solid mass was recovered and washed with distilled water for several times and then dried in oven at 80 °C for 12 h.

3.3.3. Determination of the palladium content in AT-Nano CP Pd⁰. The AT-Nano CP Pd⁰ (100 mg) was extracted with concentrated HCl (5 × 2 mL) in a screw-capped vessel, followed by treatment with concentrated nitric acid (2 mL) to digest the palladium. The mixture was then transferred into a volumetric flask (100 mL), diluted 1 : 50 for the second time and was analyzed by the ICP analysis. The loading of palladium on AT-Nano CP was estimated to be 0.2 mmol g^{–1}.⁵⁵

3.3.4. General procedure for the Sonogashira and Ullmann cross-coupling reactions. A round-bottomed flask (10 mL) was charged with aryl halides (1 mmol), phenylacetylene or phenols (1 mmol), in water (5 mL). K₂CO₃ (1.5 mmol) and the catalyst (3 mg, containing 6 × 10^{–4} mmol, 6.3 × 10^{–5} g of Pd) and the reaction mixture was stirred for the required period of time at 60 °C to reaction completion, as monitored by TLC. The reaction mixture was then cooled to room temperature, the catalyst collected by filtration, washed with water, and dried at 80 °C

and the aqueous filtrate was extracted with Et₂O (3 mL, 5 times). The organic phases were dried over anhydrous Na₂SO₄ and concentrated. The products were purified by column chromatography over silica gel using *n*-hexane–ethyl acetate (13 : 1).

4. Conclusion

In summary, the Pd⁰-nanoparticles supported on nanozeolite clinoptilolite was synthesized and characterized by different analytical techniques. Electron microscopy and N₂ adsorption–desorption data confirmed the formation of Pd⁰-nanoparticles into the pores of support. The Pd⁰-nanoparticles were spherical or ellipsoidal shape with an average diameter of 10 nm. This nanocatalyst demonstrated high catalytic activity in the Ullmann condensation and Sonogashira coupling reactions for synthesizing of the diaryl ethers and alkynes with high yields under mild reaction conditions in water. Further, the nanocatalyst was reused for eight runs without loss of activity. The key advantages of the developed method are: (i) using environmentally benign indigenous material as catalyst support, (ii) low palladium catalyst loading, (iv) facile recovery, and recycling of the catalyst and (v) copper-free, and ligand-free conditions.

Acknowledgements

This research is supported by the Islamic Azad University, Ayatollah Amoli Branch, I. R. Iran.

References

- 1 D. S. Coombs, A. Alberti, T. Armbruster, G. Artioli, C. Colella, E. Calli, J. D. Grice, F. Liebau, J. A. Mandarino, H. Minato, E. H. Nickel, E. Passaglia, D. R. Peacor, S. Quartieri, R. Rinaldi, M. Ross, R. A. Sheppard, E. Tillmanns and G. Vezzadini, *Can. Mineral.*, 1997, **35**, 1571–1606.
- 2 G. Gottardi and E. Galli, *Natural Zeolites*, Springer, New York, NY, USA, 1985.
- 3 A. Langella, M. Pansini, P. Cappelletti, B. deGennaro, M. de Gennaro and C. Colella, *Microporous Mesoporous Mater.*, 2000, **37**, 337–343.
- 4 A. Abusafa and H. Yucel, *Sep. Purif. Technol.*, 2002, **28**, 103–116.
- 5 Y. Wang, Sh. Liu, Z. Xu, T. Han, S. Chuan and T. Zhu, *J. Hazard. Mater.*, 2006, **136**, 735–740.
- 6 S. Leung, S. Barrington, S. Wan, X. Zhao and B. El-Hosseini, *Bioresour. Technol.*, 2007, **98**, 3309–3316.
- 7 Z. Özçelik, G. S. Pozan Soylu and İ. Boz, *Chem. Eng. J.*, 2009, **155**, 94–100.
- 8 S. Fozooni, N. G. Hosseinzadeh, H. Hamidian and M. R. Akhgar, *J. Braz. Chem. Soc.*, 2013, **24**, 1649–1655.
- 9 L. Yin and J. Liebscher, *Chem. Rev.*, 2007, **107**, 133–173.
- 10 M. Seki, *Synthesis*, 2006, 2975–2992.
- 11 (a) A. Biffis, M. Zecca and M. Basato, *J. Mol. Catal. A: Chem.*, 2001, **173**, 249–274; (b) J. Cejka, A. Corma and S. Zone, *Zeolites and Catalysis: Synthesis, Reactions and Applications*, Wiley-VCH, Weinheim, Germany, 2010; (c) Y. Sun, T. Sun and K. Seff, *Chem. Rev.*, 1994, **94**, 857; (d) G. A. Ozin, R. A. Prokopowicz and S. Özkar, *J. Am. Chem. Soc.*, 1992, **114**, 8953; (e) M. Zahmakıran, S. Akbayrak, T. Kodaira and S. Özkar, *Dalton Trans.*, 2010, **39**, 7521; (f) D. Azarifar and F. Soleimanei, *RSC Adv.*, 2014, **4**, 12119–12126; (g) M. Nasrollahzadeh, M. Enayati and M. Khalaj, *RSC Adv.*, 2014, **4**, 26264–26270.
- 12 (a) D. A. Kotadia, U. H. Patal, S. Gandhi and S. S. Soni, *RSC Adv.*, 2014, **4**, 32826–32833; (b) S. S. Soni and D. A. Kotadia, *Catal. Sci. Technol.*, 2014, **4**, 510–515.
- 13 K. Köhler, M. Wagner and L. Djakovitch, *Catal. Today*, 2001, **66**, 105–114.
- 14 J. Li, A. W. H. Mau and C. R. Strauss, *Chem. Commun.*, 1997, 1275–1276.
- 15 A. Biffis, M. Zecca and M. Basato, *J. Mol. Catal. A: Chem.*, 2001, **173**, 249–274.
- 16 S. Proch, Y. Mei, J. M. Rivera Villanueva, Y. Lu, A. Karpov, M. Ballauff and R. Kempe, *Adv. Synth. Catal.*, 2008, **350**, 493–500.
- 17 S. V. Ley, C. Ramarao, R. S. Gordon, A. B. Holmes, A. J. Morrison, I. F. McConvey, I. M. Shirley, S. C. Smith and M. D. Smith, *Chem. Commun.*, 2002, 1134–1135.
- 18 M. Lakshmi Kantam, K. B. Shiva Kumar, P. Srinivas and B. Sreedhar, *Adv. Synth. Catal.*, 2007, **349**, 1141–1149.
- 19 Q. Tang, Q. Zhang, P. Wang, Y. Wang and H. Wan, *Chem. Mater.*, 2004, **16**, 1967–1976.
- 20 M. Rakap and S. Özkar, *Int. J. Hydrogen Energy*, 2010, **35**, 1305–1312.
- 21 (a) F. Fu and Q. Wang, *J. Environ. Manage.*, 2011, **92**, 407; (b) S. Alexanratos, *Ind. Eng. Chem. Res.*, 2009, **48**, 388.
- 22 (a) K. Sonogashira, *J. Organomet. Chem.*, 2002, **653**, 46–49; (b) C. V. Reddy, J. V. Kingston and J. G. Verkade, *J. Org. Chem.*, 2008, **73**, 3047.
- 23 A. L. Rusanov, I. A. Khotina and M. M. Begretov, *Russ. Chem. Rev.*, 1997, **66**, 1053–1312.
- 24 K. Sonogashira, F. Diederich and P. J. Stang, in *Metal-Catalyzed Cross-Coupling Reactions*, Wiley-VCH, Weinheim, Germany, 1998, pp. 203–229.
- 25 S. N. Chen, W. Y. Wu and F. Y. Tsai, *Green Chem.*, 2009, **11**, 269–274.
- 26 S. V. Ley and A. W. Thomas, *Angew. Chem., Int. Ed.*, 2003, **42**, 5400–5449.
- 27 M. Iyoda, M. Sakaitani, H. Otsuka and M. Oda, *Tetrahedron Lett.*, 1985, **26**, 4777–4780.
- 28 R. H. F. Manske and H. L. Holmes, *The Alkaloids – Chemistry & Physiology*, Academic Press Publishers, New York, 1954, vol. 4.
- 29 J. W. Janetka and D. H. Rich, *J. Am. Chem. Soc.*, 1997, **119**, 6488–6495.
- 30 S. Tamai, M. Kaneda and S. Nakamura, *J. Antibiot.*, 1982, **35**, 1130–1136.
- 31 T. Eicher, S. Fey, W. Puhl, E. Buchel and A. Speicher, *Eur. J. Org. Chem.*, 1998, 877–888.
- 32 A. A. Moroz and M. S. Shavarstberg, *Russ. Chem. Rev.*, 1974, **43**, 679–690.
- 33 M. A. Khalilzadeh, H. Keipour, A. Hosseini and D. Zareyee, *New J. Chem.*, 2014, **38**, 42–45.

- 34 M. A. Zolfigol, V. Khakyzadeh, A. R. Moosavi-Zare, A. Rostami, A. Zare, N. Iranpoor, M. H. Beyzavi and R. Luque, *Green Chem.*, 2013, **15**, 2132–2140.
- 35 G. Evano, N. Blanchard and M. Toumi, *Chem. Rev.*, 2008, **108**, 3054–3131.
- 36 M. J. Jin and P. H. Lee, *Angew. Chem., Int. Ed.*, 2010, **49**, 1119–1122.
- 37 S. M. Baghbanian, N. Rezaei and H. Tashakkorian, *Green Chem.*, 2013, **15**, 3446–3458.
- 38 S. Brunauer, L. S. Deming, W. E. Deming and E. Teller, *J. Am. Chem. Soc.*, 1940, **62**, 1723–1732.
- 39 (a) B. J. Borah, D. Dutta, P. P. Saikia, N. C. Barua and D. K. Dutta, *Green Chem.*, 2011, **13**, 3453–3460; (b) P. P. Sarmah and D. K. Dutta, *Green Chem.*, 2012, **14**, 1086–1093.
- 40 D. Ruiz-Serrano, M. Flores-Acosta, E. Conde-Barajas, D. Ramírez-Rosales, J. M. Yáñez-Limón and R. Ramírez-Bon, *J. Mol. Struct.*, 2010, **980**, 149–155.
- 41 T. L. Barr, *Appl. Surf. Sci.*, 1983, **15**, 1.
- 42 L. Djakovitch and P. Rollet, *Adv. Synth. Catal.*, 2004, **346**, 1782–1792.
- 43 M. Choi, D. H. Lee, K. Na, B. W. Yu and R. Ryoo, *Angew. Chem.*, 2009, **121**, 3727–3730.
- 44 B. J. Borah and D. K. Dutta, *J. Mol. Catal. A: Chem.*, 2013, **366**, 202–209.
- 45 S. Banerjee, H. Khatri, V. Balasanthiran, R. T. Koodali and G. Sereda, *Tetrahedron*, 2011, **67**, 5717–5724.
- 46 P. L. Wang, L. Zhang and G. W. Wang, *Adv. Synth. Catal.*, 2012, **354**, 1307–1318.
- 47 M. Hosseini-Sarvari, Z. Razmi and M. M. Doroodmand, *Appl. Catal., A*, 2014, **475**, 477–486.
- 48 M. Nasrollahzadeha, M. Maham and M. M. Tohidi, *J. Mol. Catal. A: Chem.*, 2014, **391**, 83–87.
- 49 A. S. Roy, J. Mondal, B. Banerjee, P. Mondal, A. Bhaumik and S. M. Islam, *Appl. Catal., A*, 2014, **469**, 320–327.
- 50 L. Salvi, N. R. Davis, S. Z. Ali and S. L. Buchwald, *Org. Lett.*, 2012, **14**, 170–173.
- 51 S. Harkal, K. Kumar, D. Michalik, A. Zapf, R. Jackstell, F. Rataboul, T. Riermeier, A. Monsees and M. Beller, *Tetrahedron Lett.*, 2005, **46**, 3237–3240.
- 52 S. Jammi, S. Sakthivel, L. Rout, T. Mukherjee, S. Mandal, R. Mitra, P. Saha and T. Punniyamurthy, *J. Org. Chem.*, 2009, **74**, 1971–1976.
- 53 T. Miao and L. Wang, *Tetrahedron Lett.*, 2007, **48**, 95–99.
- 54 R. Arundhathi, B. Sreedhar and G. Parthasarathy, *Appl. Clay Sci.*, 2011, **51**, 131–137.
- 55 J. A. Albadi, M. Keshavarz, M. Abedini and M. Khoshakhlagh, *J. Chem. Sci.*, 2013, **125**, 295–298.